Can Fe isotope fractionations trace the pedogenetic mechanisms involved in podzolization?

Zuzana Fekiacova, M. L. Vermeire, Loick Bechon, J. T. Cornelis, Sophie Cornu

Can Fe isotope fractionations trace the pedogenetic mechanisms involved in podzolization?

Fekiacova, Z.[1]., Vermeire, M. L.[2], Bechon, L.[1], Cornelis, J. T.[3], Cornu, S.[1]

[1]Aix Marseille Univ, CNRS, IRD, Coll France, INRA, CEREGE, Aix-en-Provence, France

[2]Université catholique de Louvain, Earth and Life Institute, ELIe, Croix du Sud 2 bte L7.05.10, 1348 Louvain-la-Neuve, Belgium

[3]Soil-Water-Plant Exchanges, Gembloux Agro-Bio Tech, University of Liège, Belgium

*Corresponding author: Dr Zuzana Fekiacova, Email: Zuzana.Fekiacova@inra.fr, Tel.: +33 4 42 90 85 46, Fax : +33 4 42 90 85 17.

ABSTRACT

Stable Fe isotopes have shown the potential for tracing pedogenetic processes. Large isotopic fractionations were especially observed in Podzols. Nevertheless, a clear link between isotopic fractionation and elementary processes still needs to be established. To spatially distinguish the mechanisms successively involved in pedogenesis, we studied a podzolic chronosequence from Vancouver Island (British Columbia, Canada). We analyzed depth variations in soil properties (pH, particle size fractions, organic carbon, Si/Al ratio, Zr, Ti), Fe concentrations in different Fe pools, and Fe isotopic compositions. The Si/Al ratio, Zr, and Ti demonstrated that the Cox Bay Podzols developed from the same parental material, satisfying the requirements of a chronosequence. We showed that acidification, to a pH of 4.7, was a prerequisite for the start of podzolization. This first phase took place after 270 years. Furthermore, we observed that once the required pH was reached (4.7), podzolization

occurred rapidly over 50 years. We found that Fe isotope fractionation in the A/E horizon was linked to mineral dissolution, while in the podzolic B horizons this fractionation was clearly associated with the accumulation of Fe-organic complexes and poorly crystalline Fe oxyhydroxides.

1. INTRODUCTION

Iron is one of the major elements on Earth and is ubiquitous in rocks, minerals and biological samples. Stable Fe isotope analyses provide valuable information on the fate of Fe and are a promising tool for addressing questions on pedogenetic processes and soil evolution (e.g., Beard et al., 2003), particularly the identification of the mechanisms involved in a pedogenesis. While a range of isotopic variations from -0.62 to +0.72 ‰ have been documented in soils (Emmanuel et al. 2005; Fantle and DePaolo, 2004; Poitrasson et al. 2008; Thompson et al., 2007; Wiederhold et al., 2007 a, b; Fekiacova et al., 2013) no clear link between isotopic variations and pedogenetic mechanisms has yet been established. Iron isotopic fractionation related to pedogenesis is complex and is a function of the soil type. Isotopic fractionation during silicate weathering in a young ecosystem showed that a release of preferentially light Fe during silicate dissolution is a dominant mechanism and a source of light Fe for the newly formed Fe(III)-oxyhydroxides (Kiczka et al., 2010). Yet, other processes (e. g., precipitation, adsorption, organic matter complexation) are involved in soil formation and may impact the Fe isotopic signature. In particular, significant isotopic fractionation was documented in soils impacted by redox processes, i.e., Podzols and Gleysols (e.g., Fekiacova et al., 2013; Wiederhold et al. 2007 a, b).

It is generally accepted that podzolization consists of two key processes: (i) mobilization from the surface horizon and translocation of organic matter and Fe, Al, Si and (ii) immobilization and stabilization of organic matter and Fe, Al in the subsoil (e.g.,

Lunsdtröm et al., 2000; Buurman and Jongmans, 2005). Sauer et al. (2007) discussed different hypotheses on the elementary mechanisms behind these two processes. We hypothesized that Fe isotopic fractionation could be used to trace elementary mechanisms in redox processes. To do so, we needed to understand the behavior of stable Fe isotopes during podzolization.

The aim of this paper was therefore to examine the impact of different mechanisms of podzol formation on the behavior of stable Fe isotopes. To spatially distinguish the mechanisms successively involved in pedogenesis, we studied Fe isotopic fractionation along a podzolic chronosequence from Vancouver Island (British Columbia, Canada).

We first verified that the studied soils satisfied the terms of a chronosequence as defined by Sauer (2015), and demonstrated by VandenBygaart and Protz (1995), Barret and Schaetzl (1992), notably. Then, we studied the dynamics of podzolization on the basis of classical pedological data and mass balance calculations. Lastly, we linked the observed Fe isotopic variations in the Podzol depth profiles to the different soil forming mechanisms.

2. SAMPLING AND METHODS

2.1 Site and sampling

The studied soil sequence was sampled in Cox Bay, on Vancouver Island (British Columbia, Canada) and has been well characterized elsewhere (Singleton and Lavkulich 1987; Cornelis et al., 2014; Vermeire et al., 2016). The climate in this area is classified as maritime temperate, i.e. Cfb: without a dry season and with a warm summer, according to the Köppen classification (Peel et al., 2007) and is characterized by heavy mean annual precipitation (3200 mm) (Singleton and Lavkulich, 1987). Cox Bay soils developed from the beach sand, along a gentle slope: the elevational difference between any two of the sampled sites was less than 0.5 m (Singleton and Lavkulich 1987). The vegetation cover was uniform

over all sampled pits and was dominated by Sitka spruce (*Picea sitchensis*), salal (*Gaultheria shallon*) and Douglas fir (*Pseudotsuge menziesii*) (e.g., Cornelis et al., 2014). The Cox Bay beach sand is derived from the Tofino Area Graywacke Unit (Singleton and Lavkulich, 1987). The sampled soil sequence was designed to represent different stages of soil formation from the beach sand to a well-developed Podzol aged 530 years (Cornelis et al., 2014). It consisted of one beach sand sample and 5 soil pits: two Cambisol and three Podzol profiles. A 94 m long transect was designed perpendicularly to the present day shoreline. A surface age was attributed to each soil profile, using dendrochronology and geomorphology data. Tree ages were obtained using increment bores for the largest trees in the immediate vicinity of each site and by counting tree rings by Singleton and Lavkulich (1987) and by Cornelis et al. (2014). Ages obtained by Singleton and Lavkulich (1987) and Cornelis et al. (2014) are in good agreement. Taking the average rate of sand deposition into account, i.e., 0.26 m per year (Singleton and Lavkulich, 1987) and assuming a linear deposition rate with time between the successive oldest trees, a 13-m strip of active beach sand containing tree seedlings would have accumulated in approximately 50 years (Singleton and Lavkulich, 1987). Therefore 50 years were added to the tree age obtained by Cornelis et al. (2014) for each site to determine the site age. These ages range from 120 to 530 years.

The beach sand was collected on the beach and corresponds to a composite sample made of several sampling points collected down to 40 cm depth. For the soil profiles, a continuous sampling of each horizon was performed in pits.

2.2. Soil properties

Organic carbon (OC) was analyzed by dry combustion (NF ISO 10694), particle size fractions were determined by wet sieving and sedimentation separation according to Stoke's law (NF X 31-107). These analyses were performed at the Laboratoire d'Analyses des Sols

(LAS) in Arras. Soil pH was measured in 5 g : 25 ml soil : water suspension (Vermeire et al., 2016). Total Zr, Ti, Fe, Si and Al in different horizons of the Cox Bay Podzol profiles were analyzed by ICP-AES, after fusion in Li-metaborate + Li-tetraborate at 1000°C (Chao and Sanzolone, 1992) at UCL, Belgium. Total Zr and Ti are considered as immobile elements during weathering (e.g., Van Breemen and Buurman, 2002). Furthermore, in the soils, Fe is present in different forms, i.e., Fe-bearing silicate minerals and oxyhydroxides, and organic matter bound-Fe, adsorbed and exchangeable forms, which were determined using partial extractions. Pyrophosphate, oxalate (Tamm in darkness, Tamm (1922)) and dithionite-citrate-bicarbonate (DCB, Mehra and Jackson (1960)) Fe extractions were performed on bulk soil samples. We considered that (i) pyrophosphate extracted mainly adsorbed and exchangeable forms (generally negligible), organic matter-bound (OM-bound) and small Fe colloids (Jeanroy and Guillet, 1981); (ii) oxalate also extracted poorly-crystalline Fe oxide while (iii) DCB extracted in addition crystalline Fe oxide pools (Hall et al., 1996). Partial extractions of different Fe pools were performed at LAS Arras (France), with the exception of pyrophosphate extraction. Concentrations of Fe in different pools were calculated by the difference between the total Fe and the different Fe concentrations extracted. Therefore, organic matter-bound (OM-bound) and small Fe colloids correspond to the pyrophosphate fraction, poorly-crystalline Fe oxides to the difference between oxalate and pyrophosphate fractions, crystalline Fe oxides to that between DCB and oxalate fractions and silicate-bound Fe to that between total Fe and DCB fractions.

2.3. Iron isotope analyses

Iron isotopic analyses were performed on the bulk soil samples. Sample preparations were carried out in a laminar flow box, at INRA-GSE Aix-en-Provence. Approximately 250 mg of sample powder was first treated with 30% H_2O_2 in order to eliminate organic matter.

After H_2O_2 treatment, the solution was evaporated to dryness and the residue dissolved using a mixture of concentrated HF-HNO_3, followed by concentrated HCl acid, at ~130 °C. We verified that the digestion data were equivalent, within analytical error, to the total Fe concentration data obtained after fusion in Li-metaborate + Li-tetraborate at 1000°C.

The Cu-Fe fraction was isolated using the AG1X8, 200-400 mesh resin (e.g., Moynier et al., 2006). Iron was further separated and purified by anion exchange chromatography using the AG MP1, 100–200 mesh, chloride form (Maréchal et al., 1999). All reagents were ultrapure distilled acids and overall procedural blanks contained negligible quantities of Fe (< 0.1 ‰) compared to the total dissolved sample Fe content. Iron isotope analyses were performed using MC-ICPMS Neptune at the Pole Spectrometrie Ocean, Ifremer, Brest, in high-resolution mode. We used Ni (NIST 986) as an internal standard and standard-sample-standard bracketing with IRMM-014 to correct for instrumental mass discrimination. Sample solutions were diluted to match the concentration of the IRMM-014 and internal standards within 5 %, i.e. 3 ppm Fe and 4 ppm Ni. Iron isotope results are reported relative to the IRMM-014 standard using the conventional δ notation:

$$\delta^{56}Fe=[(^{56}Fe/^{54}Fe)_{sample}/(^{56}Fe/^{54}Fe)_{IRMM\text{-}014}-1]\times 1000\ (‰) \quad (1)$$

The external reproducibility (2σ) calculated on the basis of repeated measurement of the IRMM-014 standard was 0.10 and 0.16 ‰ (N = 64) for $\delta^{56}Fe$ and $\delta^{57}Fe$, respectively. In a $\delta^{57}Fe$ vs. $\delta^{56}Fe$ diagram, all soil sample measurements plot along a line with a slope of 1.44 which is equal, within error margins, to the theoretical value of ln(M57/M54)/ln(M56/M54) = 1.487, indicating mass-dependent fractionation and no influence of isobaric interferences.

2.4. Mass balance calculations

In order to investigate the dynamics of the different mechanisms involved in podzolization, i.e., acidification, organic matter accumulation and Fe mobilization (section

4.2), elemental fluxes were calculated on the basis of Brimhall's equation (Brimhall et al., 1991):

$$m_{j,\,flux} = 1/1000 \times (\rho_{ref} \times C_{j,\,ref} \times Th \times \tau_{j,\,w})/(\varepsilon_{i,\,w} + 1) \quad (2)$$

where m represents the flux of element j ($g.cm^{-2}$),

ρ_{ref} the bulk density of the reference material ($g.cm^{-3}$),

$C_{j,\,ref}$ the concentration of element j in the reference material ($g.kg^{-1}$),

Th the horizon thickness (cm),

$\tau_{j,\,w}$ the mass fraction of element j gained or lost from the weathered product with respect to the mass originally present in the reference material

and $\varepsilon_{i,\,w}$ the soil volume change over time calculated using an immobile element i.

We considered Zr (see section 2.1) as the immobile element since Ti can be mobilized through complexation with organic compounds (e.g., Cornu et al., 1999; Righi et al., 1997; Dumon and Vigneaux, 1979). The material from which the podzolization developed was taken as a reference. The elemental flux is presented as flux per cm ($m_{j,\,flux}/Th$).

3. RESULTS

3.1. Depth evolution of soil properties along the chronosequence

The evolution of pH through the studied profiles is shown in Table 1 and Figure 1. While the beach sand had basic pH (7.7), the Cambisols at pits 1 and 2 showed close to neutral pH (6), which decreased progressively towards clearly acid values, mainly lower than 5 in the upper horizon at pits 3, 4 and 5.

Total Fe concentration in the Cambisol at pit 2 and the Podzol at pit 3 was uniform with depth (Table 1, Figure 1). In the Podzols, at pits 4 and 5, we observed that upper E horizons were significantly depleted, while the subsurface Bhs horizons were significantly

enriched in Fe, compared to the deep BC-horizon (Figure 1). Similarly, we observed an accumulation of OC concentration although its maximum was recorded in the Bh while the maximum of Fe was found in the Bhs horizon. In contrast, in the Cambisol (pit 2), the maximum concentration in OC was observed in the surface horizon and decreased exponentially with depth (Figure 1). Podzol at pit 3 represents an intermediate situation with constant OC concentration in both E and Bh horizons.

In the studied chronosequence, Zr concentrations were uniform along the profiles, with the exception of the two Podzols at pits 4 and 5 that showed a significant enrichment in the upper E horizons (Table 1). For Ti, enrichment in the Bhs horizon was observed in those pits, confirming possible mobilization by organic compounds while Zr remained immobile.

In the Cox Bay soils, at pits 1 to 3, the Si/Al ratio remained stable, with an average value of 4.7. In contrast, in the Podzols at pits 4 and 5, significant enrichment was detected in the upper E horizons (Table 1).

3.2. Fe partial extractions

Significant changes were recorded vertically and laterally, in proportions of different Fe pools (Table 2, Figure 2). The Bh, Bhs and Bs horizons of pits 4 and 5 had smaller proportions of silicate-bound Fe and larger proportions of oxides and OM-bound Fe compared to the other horizons. Furthermore, E-Bh-Bhs-Bs horizons showed variations in the proportions of different Fe pools laterally along the chronosequence. Changes from pit 3 to pit 4 were restricted to the Bhs horizon (absent at pit 3), where an increase in the OM-bound and colloidal Fe pool and a respective decrease in the silicate-bound Fe pool were observed. In contrast, major variations were observed from pit 4 to pit 5: (i) in the Bh horizon, the Fe-silicates dropped from 82 to 48% while OM-bound and colloidal, poorly-crystalline and crystalline oxide pools increased from 5 to 17%, from 5 to 22% and from 8 to 13 %,

respectively; (ii) similarly, in the Bhs horizon, the Fe-silicates dropped from 61 to 39% while poorly-crystalline oxides increased from 7 to 24% and (iii) in the Bs horizon, the Fe-silicates dropped from 82 to 61% while poorly-crystalline and crystalline oxide pools increased, from 14 to 27% and from 3 to 9 %, respectively. These changes record mineral transformations during podzolization.

3.3. Fe isotopes depth evolution along the soil sequence

In the beach sand, the Cambisols at pits 1 and 2 and the Podzol at pit 3, the δ^{56}Fe had an average value of 0.13‰ with no significant variation outside analytical error (Table 1, Figure 1). In contrast, δ^{56}Fe values increased in the E horizons and decreased in the B horizons at pits 4 and 5 (Figure 1). The highest δ^{56}Fe values were observed in the E horizons and correspond to the minimum of Fe concentration. The lowest δ^{56}Fe values observed in the Bhs horizons correspond to the maximum of Fe concentration and high OC concentrations. These isotopic depth variations are in agreement with previously published data of Fe isotopes in Podzol profiles (Wiederhold et al. 2007a).

4. DISCUSSION

In the following section we discuss the evolution of the studied soil in space and time. To ensure that the Cox Bay soils satisfied the requirements of a chronosequence we first identified invariable soil forming factors and determined a reference material for podzolization for each soil pit. We then used the chronosequence to decipher the dynamics of different processes involved in podzolization. Finally, we attempted to assign Fe isotopic fractionation to a specific podzolization mechanism.

4.1. Lateral and vertical variations in the soil parent sediment prior to pedogenesis

A chronosequence is a series of soils that developed from the same parental material, vegetation, topography and climate, with pedogenesis duration being the only varying factor (e.g., Jenny 1961, Hugget, 1998, Schaetzl et al., 1994). As described above (section 2.1), distances between pits are short and the slope is gentle, thus both climate and relief can be considered as constant over the soil sequence. Nevertheless, the sediment composition may have varied over the 530 yrs of its deposition, both laterally and vertically, due to variations in proportions among different potential sources.

4.1.1. Weathering *vs* parent material source change

To assess these variations, we performed principal component analysis (PCA) considering the sand, the total Fe, Zr, Ti concentrations and the Si/Al ratios, which can be considered as a proxy for the quartz content (as quartz does not contain Al). We included in the analysis all the horizons of the studied soil profiles that experienced neither weathering nor podzolization, i.e., beach sand (BS), BC and Bw horizons (Figure 3). The first two principal components of the PCA explained 94% of the variance of the dataset. The first principal component explained 79% of the variance. This component opposed two groups of variables: the Si/Al ratios representing the quartz fraction with a loading of -0.931 and total Zr, Ti and Fe with loadings higher than 0.9 (Figure 3a). This first principal component is classically encountered in soils and is interpreted as a dilution factor by quartz contained in the sand fraction. The higher the proportion of quartz in the horizon, the lower the concentration of most elements except Si, which is the main element of quartz. This can be interpreted either as a sign of weathering or as a change in the sediment composition. Weathering would deplete the material in Fe, and enrich it in Zr and Ti, which we did not observe in the studied profiles. Instead, the Ti, Zr and Fe are strongly correlated. Thus the weathering hypothesis is unlikely. The second principal component of the PCA explained

16 % of the variance. The sand fraction was the only variable with high loading on this principal component (0.842). The two principal components identified in the PCA were interpreted as representing the evolution of the sediment composition in space and in time.

4.1.2. Evolution of parent sediment composition in space and time

We identified four different groups of observations in the space defined by the first two principal components (Figure 3b): (i) the first group formed by the beach sand alone, rich in Fe, Ti, Zr; (ii) a second group formed by the BC horizon of pit 1 and the Bw horizon of pit 2, relatively rich in Fe, Ti and Zr; (iii) a third group formed by the BC horizon of pit 2 and the BC and Bw horizons of pit 3, poor in Fe, Ti and Zr and (vi) the last group formed by the BC and Bw horizons of pits 4 and 5, and including the BC horizon of pit 3, all poor in Fe, Ti, Zr but rich in sand. On the basis of this distribution, we concluded that the parent sediment was homogeneous in the BC from pit 3 to pit 5 but different from the BC at pits 1 and 2, and from the beach sand.

The sediment from which the soils at pits 4 and 5 developed was vertically homogeneous. At pit 3, a change in the parent material composition was observed between BC and Bw horizons, the latter being closer in composition to the BC horizon at pit 2.

4.1.3. Factors influencing the evolution of parent sediment composition

It is generally accepted that the source of eroded material is the main factor controlling the sediment composition, although other parameters such as the transport history, the hydrological regime and the depositional environment can also impact sediment composition (e.g., Carter 1974). The material deposited on the beach can derive from a single source or from multiple sources. Vermeire et al. (2016) examined the C and BC horizons of the Cox Bay Podzols and found identical REE-patterns and unchanging mineralogical compositions.

They suggested that the sedimentary material came from the same source. They explained the observed variability of REE concentrations as resulting from changes in sedimentation dynamics yielding a variable content of clay, silt and sand (Vermeire et al. 2016). Such a depositional scheme has already been proposed for Barkley Sound located about 50 km SE of Cox Bay, on Vancouver Island (Carter, 1974).

All in all, we considered that the studied soil sequence fulfilled the conditions for being qualified as a chronosequence and, for the mass balance calculation, we used the BC horizon as reference material for pits 4 and 5, and the Bw horizon for pit 3.

4.2. Dynamics of different processes involved in podzolization

During podzolization, a forest development induces a decrease in pH over time and a change in the organic matter entering the soils (e.g., Koerner et al., 1997; Temminghoff et al., 1998; Cornu et al., 2009). These processes - acidification, organic matter accumulation and Fe mobilization - contribute to the differentiation of typical Podzol horizons and their duration has been explored in a few studies. Although Podzols can form over a short period, a great variability in the timespan of podzolization has been revealed (e.g., Sauer et al., 2008).

4.2.1. Dynamics of acidification

During the incipient stage of soil development, under developing coniferous vegetation, the pH of the surface horizon dropped from 8 in the beach sand to 4.6 at pit 3, over less than 270 years (Figure 4a). The drop in pH was faster from 0 (beach sand) to 120 years (pit 1) than from 120 years to 270 years (pit 3). Such a fast acidification has already been observed for soil formation from a parental material with low buffer capacity (absence of carbonates) and under coniferous trees (Stützer, 1998; Leth and Breuning-Madsen, 1992;

Crocker and Dickinson, 1957; Crocker and Major, 1955). In Cox Bay, the parent sediment is devoid of carbonates and the development of coniferous trees (*Sitka Spruce*) provides a supply of acidifying organic matter (Lindeburg et al., 2013). Similar acidification phases have been observed in Podzol chronosequences published in the literature (e.g., Sauer et al., 2008) with variable duration most likely depending on the mineral composition of the parental material.

From 270 to 530 years, the pH of the surface horizon remained stable at around 4.7 ±0.2. This stabilization of the pH corresponds to the first Podzol profile in the chronosequence. Stabilization of pH during podzolization is recorded in the literature (Sauer et al., 2008; Starr and Lindross, 2006; Righi et al., 1999; Birkeland, 1984; Bain et al., 1993; Bockheim 1980) with the exception of Caner et al. (2010). The average pH recorded at the start of podzolization was 4.2 ±0.4 (Caner et al., 2010; Sauer et al., 2008; Starr and Lindross, 2006; Righi et al., 1999). This pH corresponds to the upper limit of the Al/Fe oxide buffer range according to Stützer (1998). The pH recorded for the start of podzolization in the Vancouver Island chronosequence falls within the average range obtained for Podzol chronosequences.

4.2.2. Dynamics of organic matter accumulation

Pedogenetic evolution consists in an accumulation of OC in the upper A/E horizon up to 175 years related to the progressive installation of vegetation followed by a decrease concomitant with the formation of a weak Bh horizon (Figure 1b). In terms of elementary OC flux per cm, no significant evolution was observed over time in the surface horizon, while this flux increased in the podzolic B horizon (Bh-Bhs-Bs) from 270 years (pit 3; Figure 4b). Such evolutions have already been observed elsewhere for Podzols: for the A horizon by Schaetzl

et al. (1994) for the same duration and for A and B horizons by Sauer et al. (2008) on a longer time scale.

4.2.3. Dynamics of Fe mobilization

The major Fe transfers evidenced by decreasing Fe_{DCB} concentration in the E horizon and accumulation of Fe_{DCB} in the Bhs horizon started at 270 years (pit 3, Figure 4c). This evolution, synchronized with an increase in OC in the B horizon, marks the beginning of podzolization from 270 to 335 years as demonstrated by the strong correlation between elementary OC and Fe_{DCB} fluxes in the B horizons (R^2=0.99, n=3, correlation significant at 1% confidence level). This correlation was already observed in other Podzols (e.g., Eusterhues et al., 2005). Once the required pH has been reached, podzolization starts within 50 years. Sauer et al. (2008) compiled data on incipient podzolization and showed that it is generally recorded within 200-500 years. However, this duration includes the initial acidification phase. More rapid cases of incipient podzolization were observed, e.g., 60 years (Cornu et al., 2008) and 144 years (Caner et al., 2010), due to faster acidification. In the case studied by Cornu et al. (2008), the chronosequence started from a mature Cambisol, instead of a parental material, explaining the rapid start of podzolization. The duration, i.e. the timespan between the last non-podzolic and the first podzolic profile, observed by Cornu et al., (2008) is comparable to that obtained in this study, or that observed by Caner et al. (2010).

The removal of Fe_{DCB} from the E horizon (Figure 4c), corresponds to the removal of crystalline Fe oxides but is accompanied by a large removal of silicate-bound Fe (Figure 5a), from hornblende, augite and chlorite that are weathered in the E horizon (Vermeire et al., 2016). Accumulation of Fe_{DCB} in the B podzolic horizons (Figure 4c) can be explained by a positive flux of OM-bound and colloidal Fe in the Bhs horizon at 335 (pit 4) and 530 years (pit 5) and a small positive flux in crystalline Fe oxides at 530 years (pit 5) in the same

horizon (Figure 5b). Likewise, a loss of Fe is recorded at both 335 and 530 years. These results are in agreement with Caner et al. (2010) who observed changes in silicate mineralogy, in both E and B horizons, and an increase in both oxalate and DCB Fe concentrations in the B horizon on the same time step. Rapid silicate transformations in Podzols were also recorded elsewhere (see the compilation by Cornu et al., 2012; Cornelis et al., 2014).

4.3. Fe isotopic fractionation as a function of the different podzolization mechanisms

Wiederhold et al. (2007a) interpreted the isotopic variation observed in two Podzol profiles sampled at two different locations in Germany as related to Fe mobilization, yet they offered no information on the timescale of the podzolization process. Our study on the Cox Bay chronosequence provides new input for the understanding of Fe isotope fractionation during podzolization.

No isotopic variations, outside analytical error, were observed during the first 270 years, indicating that acidification and OC accumulation had no impact on the isotopic composition of the Fe-bearing phases (Figure 5). From 270 to 335 years, significant changes marked Fe isotopic profiles and the observed isotopic patterns were similar to those described by Wiederhold et al. (2007a). The increase in δ^{56}Fe values in the E horizon and a negative flux of silicate bound-Fe and crystalline Fe oxides (Figure 5a) are consistent with the concept of light Fe removal due to mineral dissolution and down-profile translocation. Furthermore, a decrease in δ^{56}Fe values simultaneous to the positive flux of OM-bound and colloidal Fe pool in the Bhs horizon, from 270 to 335 years (Figure 5b), indicates preferential accumulation of light Fe in this horizon. These light δ^{56}Fe values were associated with a maximum of OM-bound and colloidal Fe, and of poorly crystalline Fe oxides (Figure 2), suggesting that light Fe accumulation is predominantly due to precipitation of these Fe pools in the Bhs horizon (pit 4, 5). These data are in agreement with the interpretation of Wiederhold et al. (2007a) who

suggested that the total Fe isotopic pattern in the Podzol profile is driven by the isotopic signature of the poorly crystalline Fe oxides. Nevertheless, the observed light Fe enrichment in the German Podzols was significantly larger than that found in our Podzols. This discrepancy could result from an age difference. In the absence of isotopic data on older Cox Bay profiles, however, no firm conclusion can be drawn.

4. CONCLUSIONS

Previously published literature indicated that podzolization is a rapid process. We therefore chose a unique chronosequence composed of 5 soil profiles developed within a short duration, from 120 to 530 years, in order to spatially distinguish the mechanisms successively involved in Podzol formation. We showed that:

i. Acidification to a pH of around 4.5 is a prerequisite for the start of podzolization. This initial phase is due to the accumulation of organic matter in the surface horizon and precedes the mobilization of organic matter and Fe. In the Cox Bay chronosequence, this phase took 270 years, which is the duration classically observed in the literature.

ii. Once the threshold pH value has been reached, OC and Fe mobilization and accumulation are triggered rapidly, in less than 50 years. Iron is mainly accumulated as organic complexes over the first 150 years and then as pedogenic Fe oxides. As shown in the literature, Fe accumulation can continue over several thousands of years. The absence of soil profiles older than 530 years in Cox Bay prevented further discussion on this point.

iii. Iron isotopic fractionation in the upper A/E horizon was linked to mineral dissolution. Preferential release of light Fe isotopes from the silicate minerals resulted in enrichment of heavy Fe isotopes and positive δ^{56}Fe values (0.25 ‰) in this horizon. We hypothesize that the intensity of this fractionation may be related to the nature of the weathered silicates.

iv. Iron isotopic fractionation in the podzolic B horizons was clearly associated with the accumulation of Fe-organic complexes and poorly crystalline Fe oxyhydroxides. Light Fe enrichment was measured in the illuvial Bh-Bhs horizons, where the accumulation of secondary Fe phases was maximal. Whether this enrichment was due to (i) the preferential input of light Fe coming from the surface, (ii) a preferential incorporation of light Fe in the secondary Fe phases or (iii) a preferential complexation of light Fe by the OM, still remains to be elucidated .

For future investigations, we suggest that Fe isotopic studies should be coupled with mineral separations and characterization. We believe that physical separation of different mineral pools could help unravel the Fe isotope signatures of individual solid phases. In addition, we suggest that to gain greater insight into the dynamics of the subsequent mechanisms, it would be necessary, in future studies, to use a chronosequence that spans over thousands of years, but with detailed sampling over the early stages of podzolization.

Acknowledgments

We thank Bernard Angeletti from CEREGE (UMR 7330 Aix Marseille Université - CNRS) for his help with the ICP MS, Emmanuel Ponzevera from the Pole Spectrometrie Ocean, Ifremer, Brest for his help with the Neptune MC-ICP-MS analyses and INRA for financial support for this project. We also thank Anne Iserentant and the Soil Science and Environment Geochemistry lab of the Earth and Life institute (Université catholique de Louvain, Belgium) for the analysis with the ICP-AES. Financial support was also provided by the Fonds de la Recherche Scientifique (F.R.S.-FNRS, Belgium), through a FRFC project.

References

Bain, D.C., Mellor, A., Robertson-Rintoul, M.S.E., Buckland, S. T., 1993. Variations in weathering processes and rates with time in a chronosequence of soils from Glen Feshie, Scotland. Geoderma 57, 275-293.

Barrett, L.R. and R.J. Schaetzl. 1992. An examination of podzolization near Lake Michigan using chronofunctions. Can. J. Soil Sci. 72:527-541.

Beard, B.L., Johnson, C.M., Skulan, J.L., Nealson, K.H., Cox, L., Sun, H., 2003. Application of Fe isotopes to tracing the geochemical and biological cycling of Fe. Chem. Geol. 195, 87–117.

Birkeland, P.W., 1984. Soil-geomorphic research - a selective overview. Geomorphology 3, 207-224.

Brimhall, G. H., Lewis, C.J., Ford, C., Bratt, J., Taylor, G., Warin, O., 1991. Quantitative geochemical approach to pedogenesis: importance of parent material reduction, volumetric expansion, and eolian influx in lateritization. Geoderma 51, 51-91.

Bockheim, J.G. 1980. Solution and use of chronofunctions in studying soil development. Geoderma 24:71-85.

Buurman, P., Jongmans, A.G., 2005. Podzolisation and soil organic matter dynamics. Geoderma 125, 71-83.

Caner, L., Joussein, E., Salvador-Blanes, S., Hubert, F., Schlicht, J.-F., Duigou, N., 2010. Short-time clay-mineral evolution in a soil chronosequence in Oléron Island (France). J. Plant Nutr. Soil Sci. 173, 591-600.

Carter, L., 1974. An evaluation of the provenance of terrigenous sediments from offshore Vancouver Island. Can. J. Earth Sci. 11, 664-676.

Chao, T.T., Sanzolone, R.F., 1992. Decomposition techniques. J. Geochem. Explor. 44, 65-106.

Cornelis, J.T., Weis, D., Lavkulich, L., Vermeire, M.L., Delvaux, B., Barling, J., 2014. Silicon isotopes record dissolution and re-precipitation of pedogenic clay minerals in a podzolic soil chronosequence. Geoderma 235-236, 19-29.

Cornu, S., Montagne, D., Hubert, F., Barré, P., Caner, L., 2012. Evidence of short-term clay evolution in soils under human impact. C. R. Geoscience 344, 747–757.

Cornu, S., Montagne, D., Vasconcelos, P. M., 2009. Dating constituent formation in soils to determine rates of soil processes: A review. Geoderma 153, 293-303.

Cornu, S., Besnault, A., Bermond, A., 2008. Soil podzolization induced by deforestation as shown by sequential and kinetic extractions of Fe and Al. Eur. J. Soil Sci. 59, 222-232.

Cornu, S., Lucas, Y., Lebon, E., Ambrosi, J.P., Luizão, F., Rouiller, J., Bonnay, M., Neal, C., 1999. Evidence of titanium mobility in soil profiles, Manaus, central Amazonia. Geoderma 91, 281-295.

Crocker, R.L. and J. Major. 1955. Soil development in relation to vegetation and surface age at Glacier Bay, Alaska. J. Ecol. 43:427-448.

Crocker, R.L. and B.A. Dickinson. 1957. Soil development on the recessional moraines of the Herbert and Mendenhall glaciers, southeastern Alaska. J. Ecol. 45:169-185.

Dumon, J.C., Vigneaux, M., 1979. Evidence for some mobility of titanium in podzols and under laboratory conditions as a result of the action of organic agents. Phys. Chem. Earth 11, 331-337.

Eusterhues, K. Rumpel, C., Kogel-Knabner, I., 2005. Organo-mineral associations in sandy acid forest soils: importance of specific surface area, iron oxides and micropores. Eur. J. Soil Sci. 56, 753-763.

Emmanuel, S., Erel, Y., Matthews, A., Teutsch, N., 2005. A preliminary mixing model for Fe isotopes in soils. Chem. Geol. 222, 23–34.

Fantle, M.S., DePaolo, D.J., 2004. Iron isotopic fractionation during continental weathering. Earth Planet. Sci. Lett. 228, 547–562.

Fekiacova, Z., Pichat, S., Cornu. S., Balesdent, J., 2013. Inferences from the vertical distribution of Fe isotopic compositions on pedogenetic processes in soils. Geoderma 209-210, 110-118.

Hall G.E.M., Vaive, J. E., Beer, R., Hoaschi, M. 1996. Selective leaches revisited, with emphasis on the amorphous Fe oxyhydroxides phase extraction. J. Geochem. Explor. 56, 59-78.

Hugget, R.J., 1998. Soil chronosequences, soil development, and soil evolution: a critical review. Catena 32, 155-172.

Jeanroy, E., Guillet, B., 1981. The occurrence of suspended ferruginous particles in pyrophosphate extracts of some soil horizons. Geoderma 26, 95-105.

Jenny, H., 1961. Derivation of State Factor Equations of Soils and Ecosystems. Soil Sci. Soc. Proc., 385-388.

Kiczka, M., Wiederhold, J.G., Frommer, J., Kraemer, S. M., Bourdon, B., Kretzschmar, R., 2010. Iron isotope fractionation during proton- and ligand-promoted dissolution of primary phyllosilicates. Geoch. Cosmochim. Acta 74, 3112-3128.

Koerner, W., Dupouey, J. L., Dambrine, E., Benoît, M., 1997. Influence of past land use on the vegetation and soils of present day forest in the Vosges mountains, France. J. Ecol. 85, 351-358.

Leth, S., Breuning-Madsen, H., 1992. Changes in soil profile development and nutrient status due to the afforestation of agricultural land. Geografisk Tidsskrift-Dan. J. Geogr. 92:1, 70-74.

Lindeburg, K.S., Almond, P., Roering, J.J., Chadwick, O.A., 2013. Pathways of soil genesis in the Coast Range of Oregon, USA. Plant and Soil, 367, 57-75.

Lundström, U.S., van Breemen, N., Bain, D., 2000. The podzolization process. A review. Geoderma 94, 91-107.

Maréchal, C.N., Télouk, P., Albarède, F., 1999. Precise analysis of copper and zinc isotopic compositions by plasma-source mass spectrometry. Chem. Geol. 156, 251-273.

Mehra, O.P., Jackson, M.L., 1960. Iron oxide removal from soils and clays by a dithionite-citrate system buffered with sodium bicarbonate. Clays Clay Miner., 7, 317-327.

Moynier, F., Albarède, F., Herzog, G.F., 2006. Isotopic composition of zinc, copper, and iron in lunar samples. Geoch. Cosmochim. Acta 70, 6103-6117.

Peel, M.C., Finlayson, B.L., McMahon, T.A., 2007. Updated world map of the Köppen-Geiger climate classification. Hydrology and Earth System Sciences. 11, 1633–1644.

Poitrasson, F., Viers, J., Martin, F., Braun, J.J., 2008. Limited iron isotope variation in recent lateritic soils from Nsimi, Cameroon: implications for the global Fe geochemical cycle. Chem. Geol. 253, 54–63.

Righi, D., Räisänen M.L., Gillot, F., 1997. Clay mineral transformations in podzolized tills in central Finland. Clay miner. 32, 531-544.

Righi, D., Huber, K., Keller, C., 1999. Clay formation and podzol development from postglacial moraines in Switzerland. Clay Miner 34, 319-332.

Sauer, D., Sponagel, H., Sommer, M., Giani, L., Jahn, R., Stahr, K., 2007. Podzol: Soil of the year 2007. A review on its genesis, occurrence, and functions. Journal of Plant Nutrition and Soil Science, 170, 581-597.

Sauer, D., Schülli-Maurer, I., Sperstad, R., Soerensen, R. Stahr, K., 2008. Podzol development with time in sandy beach deposits in southern Norway. J. Plant Nutr. 171, 483-497.

Sauer, D., 2015. Pedological concepts to be considered in soil chronosequence studies. Soil Res. 53, 577-591.

Schaetzl, R.J., Barrett, L.R., and J.A. Winkler. 1994. Choosing models for soil chronofunctions and fitting them to data. Eur. J. Soil Sci. 45:219-232.

Singleton, G.A., Lavkulich, L.M., 1987. A soil chronosequence on beach sands, Vancouver Island, British Columbia. Can. J Soil Sci. 67, 795-810.

Starr, M., Lindross, A.-J., 2006. Changes in the rate of release of Ca and Mg and normative mineralogy due to weathering along a 5300-year chronosequence of boreal forest soils. Geoderma 133, 269-280.

Stützer, A., 1998. Early stages of podzolisation in young aeolian sediments, western Jutland. Catena 32, 115-129.

Tamm, O., 1922. Eine Method zur Bestimmung der anorganishen Komponenten des Golkomplex in Boden. Medd. Statens skogforsoksanst, 19, 385-404.

Temminghoff. E. J. M., van der Zee, S. E. A. T. M., De Haan, F. A. M., 1998. Effect of dissolved organic matter on the mobility of copper in a contaminated sandy soil. Eur J. Soil Sci. 49, 617-628.

Thompson, A., Ruiz, J., Chadwick, O.A., Titus, M., Chorover, J., 2007. Rayleigh fractionation of iron isotopes during pedogenesis along a climatic sequence of Hawaiian basalts. Chem. Geol. 238, 72–83

van Breemen, N., Buurman, P., 2002. Soil Formation. Second Edition ed. Kluwer Academic Publishers, Netherlands.

VandenBygaart, A.J. and R. Protz. 1995. Soil genesis on a chronosequence, Pinery Provincial Park, Ontario. Can. J. Soil Sci. 75:63-72.

Vermeire, M.L., Cornu, S., Fekiacova, Z., Detienne, M. Delvaux, B., Cornelis, J.T., 2016. Rare Earth Elements dynamics along pedogenesis in a chronosequence of podzolic soils. Chem. Geol. 446, 163-174.

Wiederhold, J.G., Teutsch, N., Kraemer, M., Halliday, A.N., Kretzschmar, R., 2007a. Iron isotope fractionation in oxic soils by mineral weathering and podzolization. Geoch. Cosmochim. Acta 71, 5821-5833.

Wiederhold, J.G., Teutsch, N., Kraemer, M., Halliday, A.N., Kretzschmar, R., 2007b. Iron isotope fractionation during pedogenesis in redoximorphic soils. Soil Sci. Soc. Am. J. 71, 1840–1850.

Table and figure captions

Table 1: Pedological data, Fe isotopic compositions and concentrations of total Fe in the Cox Bay Podzols. Particle size distribution and organic C (OC) were determined at the Laboratoire d'Analyses des Sols (LAS) Arras.

Table 2: Concentrations of different Fe pools in the Cox Bay Podzols.

Figure 1: Total Fe (a) and organic C (OC) (b) concentrations, pH (c) and Fe isotopic compositions (d) in the Cox Bay soils. Error bars in δ^{56}Fe plots represent the 2σ. Error bars in Fe tot and OC plots correspond to 5%.

Figure 2: Variations in the proportions of different Fe pools in pits 2, 3, 4 and 5 of the Cox Bay soils. For convenience, the proportions are reported as numbers over each bar.

Figure 3: Results of the principal component analysis performed on the beach sand (BS), BC and Bw horizons of the studied soil profiles. (a) Variable space, (b) Observation space.

Figure 4: Variation with time of (a) pH in the surface A/E horizons, (b) OC flux/cm and (c) DCB extracted Fe flux/cm in the surface A/E and subsurface B horizons of the Cox Bay soils. Grey fields indicate the time span (<50 years) of OC accumulation and Fe mobilization, triggered after the pH threshold was reached.

Figure 5: Variations with time of the Fe isotopic composition and of the Fe flux/cm of the different individual Fe pools, i.e., OM bound and colloidal Fe, poorly crystalline Fe oxides, crystalline Fe oxides and silicate-bound Fe in (a) the surface A/E and (b) deep Bhs horizons.

Pit number	Soil type	Age, years	Horizon	Sampling depth, cm	δ^{56}Fe ±2σ, ‰	Fe tot, g.kg^{-1}	pH_{water}	OC, g.kg^{-1}	Clay, g.kg^{-1}	Silt, g.kg^{-1}	Sand, g.kg^{-1}	Si/Al	Zr tot, g.kg^{-1}	Ti tot, g.kg^{-1}
0	Beach sand	0	C	0 - 40	0.15 ± 0.06	48.92	7.7	0.94	22	8	970	3.8	0.23	7.14
1	Cambisol	120	BC	0 - 75	0.13 ± 0.01	34.64	5.9	4.65	25	17	958	4.1	0.12	4.39
2	Cambisol	175	E	0 - 3	nd	29.70	5.4	34.10	41	63	896	nd	0.12	4.46
			Bw	3 - 44	0.15 ± 0.08	33.62	5.8	4.28	21	20	959	4.4	0.09	4.10
			BC	44 - 75	nd	25.00	5.9	2.44	21	9	970	4.8	0.07	2.95
3	Podzol	270	E	0 - 7	0.11 ± 0.07	18.99	4.6	17.00	43	40	917	5.4	0.08	2.87
			Bh	7 - 23	0.05 ± 0.11	20.67	5.1	18.60	10*	17*	972*	5.1	0.06	2.33
			Bw	23 - 57	0.16 ± 0.08	18.43	5.3	11.60	16	7	977	5.5	0.08	2.20
			BC	57 - 75	0.15 ± 0.04	25.87	5.4	8.33	9	8	983	4.7	0.07	3.02
4	Podzol	335	E	0 - 10	0.20 ± 0.04	10.81	4.9	8.73	50	133	817	6.7	0.20	3.39
			Bh	10 - 17	0.14 ± 0.14	25.29	5.5	21.30	24	29	947	4.8	0.09	3.50
			Bhs	17 - 18	-0.02 ± 0.11	37.76	nd	17.30	nd	nd	nd	4.5	0.08	3.67
			Bs	18 - 23	0.10 ± 0.10	31.18	5.3	5.03	10	19	971	4.4	0.08	3.59
			Bw	23 - 63	0.11 ± 0.08	25.27	5.4	3.06	8	11	981	4.8	0.10	3.04
			BC	63 - 113	0.13 ± 0.01	24.87	5.3	1.95	7	7	986	5.0	0.07	3.01
5	Podzol	530	E	0 - 8	0.25 ± 0.04	10.66	4.5	21.40	53	179	768	8.9	0.23	3.11
			Bh	8 - 9.5	0.14 ± 0.10	19.55	4.5	33.40	94	114	792	6.1	0.19	4.17
			Bhs	9.5 - 10	0.00 ± 0.05	39.25	4.5	32.80	nd	nd	nd	5.4	0.08	4.36
			Bs	10 - 15	0.10 ± 0.01	29.29	4.8	12.50	17	35	948	4.8	0.07	3.00
			Bw	15 - 40	0.19 ± 0.10	26.79	5.0	1.46	15	7	978	4.8	0.07	3.21
			BC	40 - 60	0.09 ± 0.10	26.28	5.1	0.78	3	6	991	4.9	0.07	3.09

Data for Fe isotopic compositions are from this work. Total Fe (the fusion data), Zr, Ti, Si, Al concentrations and pH are from Vermeire et al. (2016). nd = not determined, * data from Cornelis et al. (2014)

Table 1

Pit number	Soil type	Age, years	Horizon	Sampling depth, cm	Fe_{pyro}, $g.kg^{-1}$	$Fe_{oxalate}$, $g.kg^{-1}$	Fe_{DCB}, $g.kg^{-1}$
0	Beach sand	0	C	0 - 40	0.03	7.61	7
1	Cambisol	120	BC	0 - 75	0.51	3.16	4.29
2	Cambisol	175	E	0 - 3	0.72	2.14	3.87
			Bw	3 - 44	0.66	2.96	3.98
			BC	44 - 75	0.30	2.54	3.29
3	Podzol	270	E	0 - 7	0.87	1.92	3.15
			Bh	7 - 23	1.42	2.86	3.69
			Bw	23 - 57	1.17	2.7	3.58
			BC	57 - 75	0.85	2.94	3.86
4	Podzol	335	E	0 - 10	0.63	1.07	1.54
			Bh	10 - 17	1.33	2.54	4.5
			Bhs	17 - 18	9.96	12.5	14.8
			Bs	18 - 23	0.29	4.57	5.54
			Bw	23 - 63	0.09	3.29	4.08
			BC	63 - 113	0.05	2.68	3.29
5	Podzol	530	E	0 - 8	0.47	0.88	1.9
			Bh	8 - 9.5	3.29	7.65	10.1
			Bhs	9.5 - 10	12.44	21.8	24.1
			Bs	10 - 15	0.85	8.89	11.5
			Bw	15 - 40	0.03	3.16	3.72
			BC	40 - 60	0.02	2.63	3.14

Partial extractions of Fe-oxalate (Feoxalate) and Fe-DCB (FeDCB) were performed at LAS Arras. Pyrophosphate extraction (Fepyro) data are from Vermeire et al., 2016.
nd = not determined

Table 2

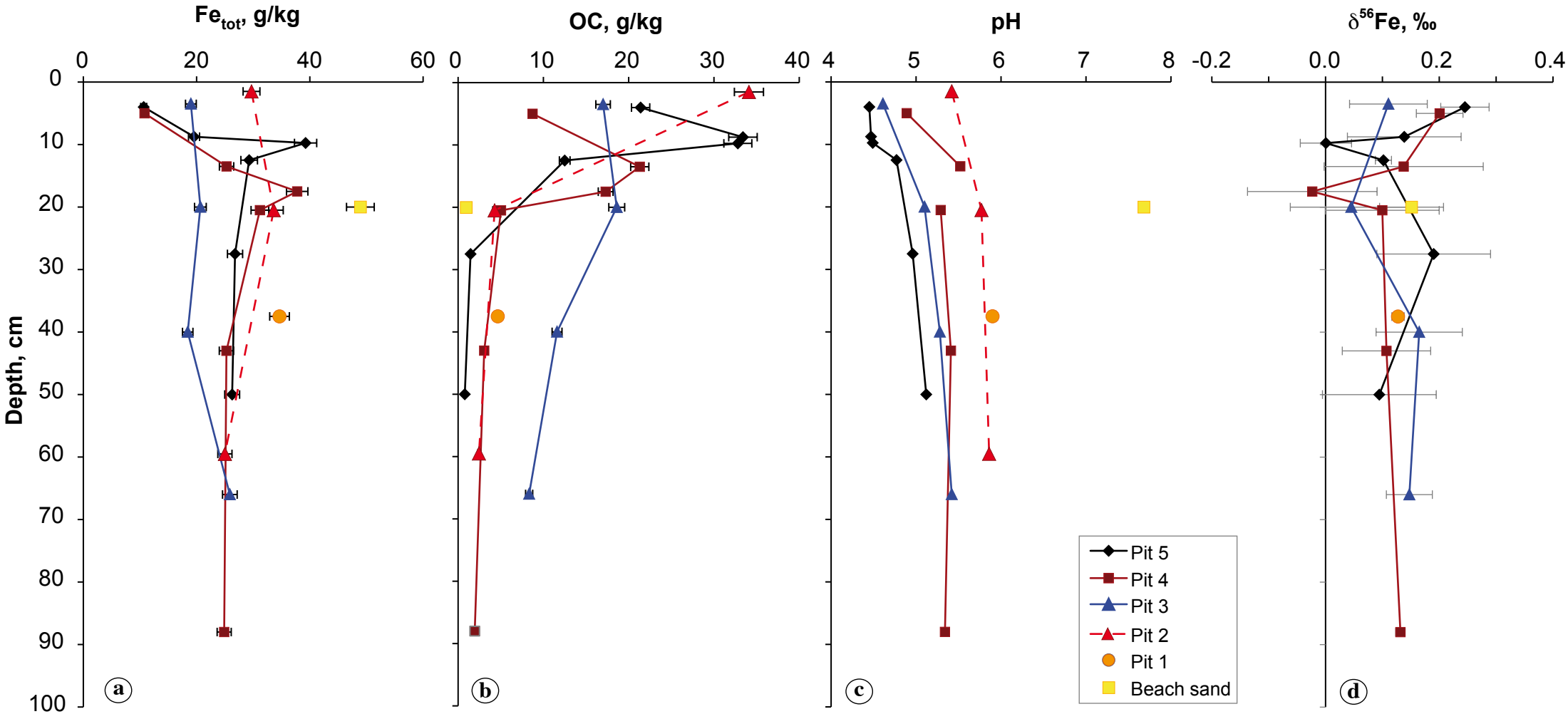
Fe$_{tot}$, g/kg
OC, g/kg
pH
δ^{56}Fe, ‰
Depth, cm
0
10
20
30
40
50
60
70
80
90
100
a
b
c
d
Pit 5
Pit 4
Pit 3
Pit 2
Pit 1
Beach sand

Figure 1

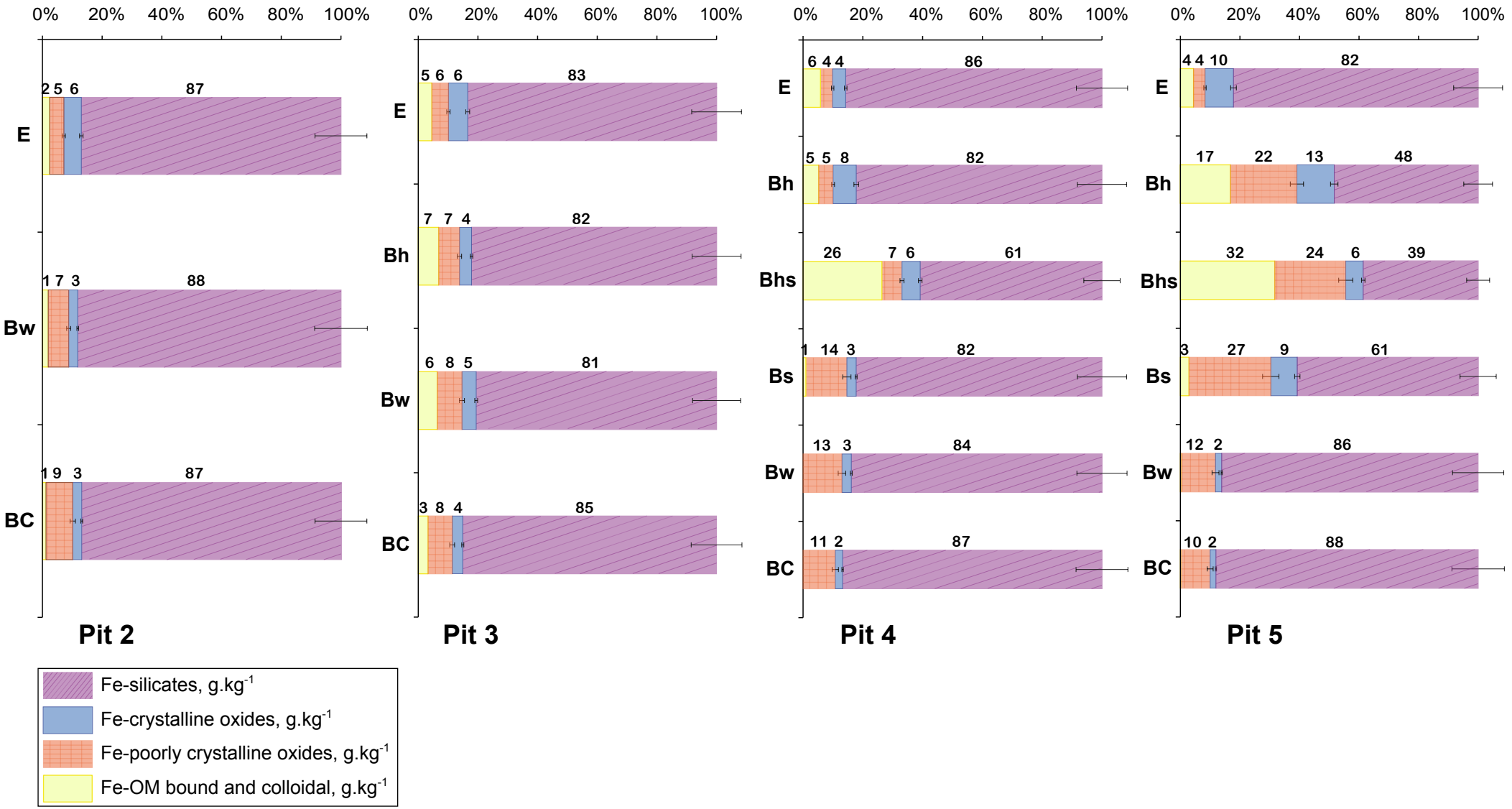
0%
20%
40%
60%
80%
100%
E
Bw
BC
2 5 6
87
1 7 3
88
1 9 3
87
Pit 2
Bh
Bs
Bhs
5 6 6
83
7 7 4
82
6 8 5
81
3 8 4
85
Pit 3
6 4 4
86
5 5 8
82
26 7 6
61
1 14 3
82
13 3
84
11 2
87
Pit 4
4 4 10
82
17 22 13 48
32 24 6 39
3 27 9 61
12 2
86
10 2
88
Pit 5
Fe-silicates, g.kg-1
Fe-crystalline oxides, g.kg-1
Fe-poorly crystalline oxides, g.kg-1
Fe-OM bound and colloidal, g.kg-1

Figure 2

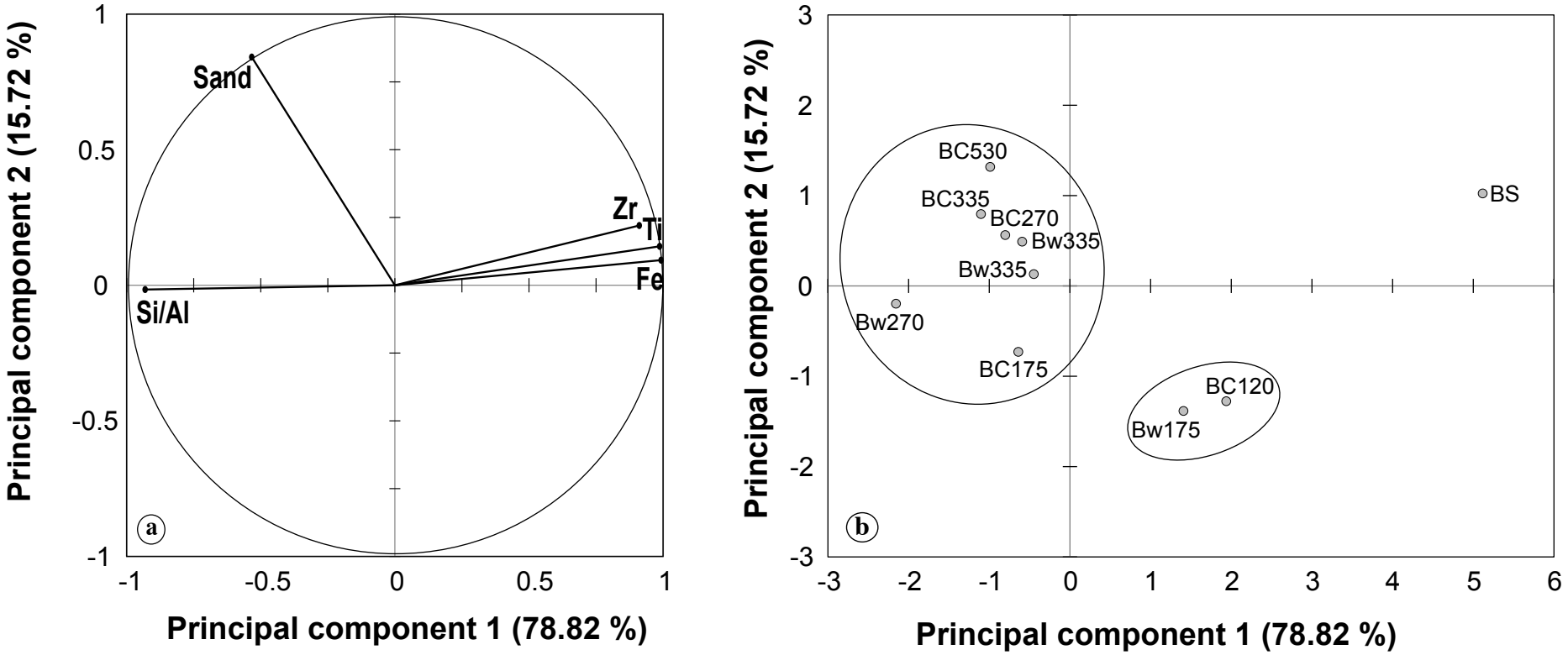
Principal component 2 (15.72 %)
Principal component 1 (78.82 %)
Sand
Zr
Ti
Fe
Si/Al
a
BC530
BC335
BC270
Bw335
Bw335
Bw270
BC175
BS
BC120
Bw175
b

Figure 3

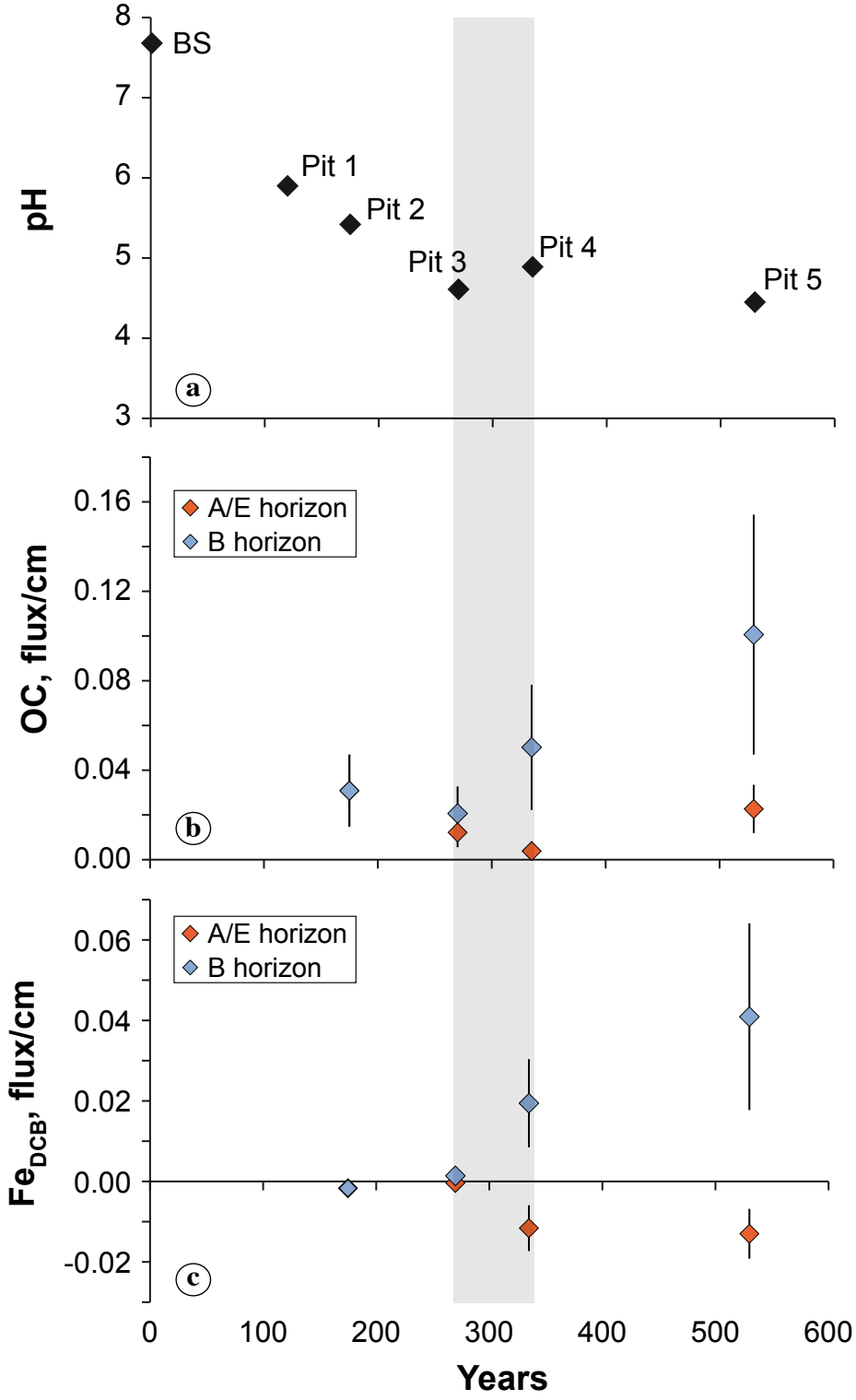
pH
BS
Pit 1
Pit 2
Pit 3
Pit 4
Pit 5
a
OC, flux/cm
A/E horizon
B horizon
b
Fe_{DCB}, flux/cm
A/E horizon
B horizon
c
Years

Figure 4

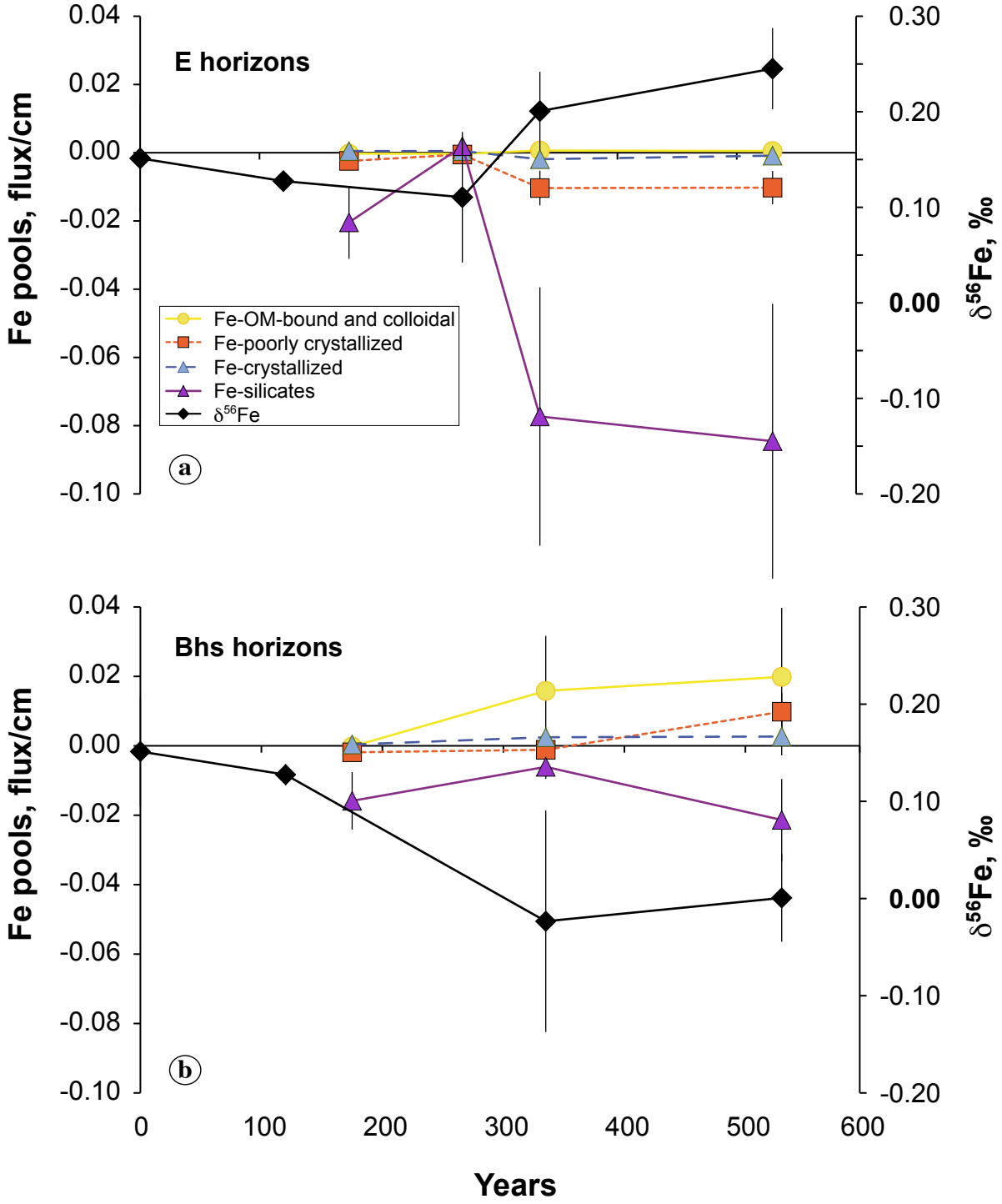
E horizons
Bhs horizons
Fe pools, flux/cm
δ56Fe, ‰
Fe-OM-bound and colloidal
Fe-poorly crystallized
Fe-crystallized
Fe-silicates
δ56Fe
a
b
0.04
0.02
0.00
-0.02
-0.04
-0.06
-0.08
-0.10
0.30
0.20
0.10
0.00
-0.10
-0.20
0
100
200
300
400
500
600
Years

Figure 5